Effects of ported shroud casing treatment on the acoustic and flow behaviour of a centrifugal compressor

Journal Title
XX(X):1–15

DOI: 10.1177/ToBeAssigned
www.sagepub.com/
SAGE

Sidharath Sharma[1], Jorge García-Tíscar[2], John M. Allport[1], Simon Barrans [1], and Ambrose K. Nickson[3]

Abstract

Centrifugal turbomachines of smaller sizes operating at higher speeds have become pervasive due to the increased specific power and reliability achieved by improvements in manufacturing, materials and computational methods. The presence of these small turbomachines, specifically compressors, in helicopters, unmanned aerial vehicles (UAVs), auxiliary power units (APUs), turbochargers and micro gas turbines necessitates superior aerodynamic performance over a broad operational range which is widely achieved by ported shroud casing designs. In addition to aerodynamic performance, acoustic emissions have become a critical aspect of design for these small centrifugal compressors due to high operational speeds. Furthermore, the literature on the acoustic effects of the casing treatment is rather limited. Therefore, the impact of ported shroud casing treatment on the acoustic and flow features of the compressor operating at the design and near surge conditions have been quantified by numerically modelling the open and blocked configuration of the compressors. Upon comparing with experimental results, the numerical spectra are shown to capture the differences between the two configurations at the investigated operating points with reasonable accuracy. Although the casing treatment is generally seen to decrease the overall acoustic emission of the compressor at both operating conditions, increased propagation of tonal content in the direction upstream to the impeller is observed, particularly for design operation. Broadband characteristics in the lower and medium frequency regions usually associated with near surge operation including 'whoosh' noise are observed to be alleviated by the ported shroud casing treatment.

Keywords

Compressor noise, SBES, Ported shroud, CFD, Aeroacoustics

Introduction

Ported shroud (PS) casing treatment is one of the most widely used passive flow control[1–3] strategies in centrifugal compressors for delaying the onset of surge by recirculating the low momentum fluid that blocks the blade passage back to the compressor inlet and thereby, enhancing the stable flow region of the compressor operation – without requiring the control logic[4] of active devices such as variable geometries. A number of investigations in the past[3] and recent times[5] are focused on understanding the mechanism of these recirculation losses and potential means to minimise them. The other, less researched aspect of the ported shroud design is its impact on the acoustics of the compressor.

The early work on the acoustics of small centrifugal compressors was driven by automotive and turbocharger manufactures given the product sensitivity to the acoustic emission, specifically to broadband noises identified by an onomatopoeia like 'whoosh'[6,7] noise. The experimental investigations of Evans and Ward[7] and Trochon[8] presented the 1.5-3 kHz range for whoosh noise while the work of Teng and Homco[6] and Figurella

[1] Turbocharger Research Institute, University of Huddersfield, UK
[2] CMT – Motores Térmicos, Universitat Politècnica de València, Spain
[3] BorgWarner Turbo Systems Division, UK

Corresponding author:
Sidharath Sharma, Turbocharger Research Institute
University of Huddersfield, Queensgate, Huddersfield, HD1 3DH, UK.

Email: sidharath.sharma@hud.ac.uk

et al.[9] provided an inclusive frequency range of 4-12 kHz for the whoosh noise. An inclusive frequency range is used by some authors[6,9] to identify broadband characteristics by conflating 'whoosh' noise which is observed within plane wave range with the so called Tip Clearance Noise (TCN)[10,11] seen outside the plane wave region. Furthermore, tonal features like Rotating Order (RO) tones or 'buzz-saw' tones[10,12] and Blade Pass Frequency (BPF) are consistently identified in literature and are shown to be associated with the sonic conditions[12] at the leading edges of the impeller.

Mendonça et al.[13] presented a numerical campaign to model the acoustic characteristics of the compressor which served as the basis for the investigations of Broatch et al.[14,15]. Furthermore, an exhaustive evaluation of the various numerical parameters for predicting flow-induced noise in compressors is presented by Sharma et al.[16]. Researchers at KTH[5,17,18] numerically investigated a compressor with PS casing treatment to gain insights into the flow dynamics specifically near surge and complimented the results with flow visualisation data[19] acquired using Particle Image Velocimetry (PIV).

The literature on the acoustic impact of casing treatment is scarce, and the general perception[20,21] is that the casing treatment deteriorates the acoustic spectra of the compressor. Chen and Yin[20] and Chen and Lei[21] pointed out the 'noise issue', specifically BPF, as the reason for the limited use of casing treatment in the compressors used in the turbochargers of passenger cars without providing any evidence for these claims.

Recent studies[22,23] on the acoustic impact of casing treatments presented some interesting and contrary results. Dehner et al.[22] experimentally investigated the impact of PS casing treatment and observed a decrease in the overall noise levels at the inlet duct for design operation despite increased tonal content by using casing treatment. For near surge or low flow conditions, an increase in the overall noise levels was seen at the inlet. The spectrum measured at the outlet duct for the PS compressor showed little difference at near surge conditions while a decrease was again seen at the design conditions. It is worth pointing out that the casing treatment used in this work decreased the stable flow region of the compressor rather than increasing it. Fardafshar and Koutsovasilis[23] explored the impact of the PS by modelling the near-field spectra of compressors with and without casing treatment at near surge and choke conditions. The results showed higher noise levels for the compressor without casing treatment for near surge operation while lower noise levels for the same compressor were seen for choke operation. The current investigation aims to further understand the impact of the casing treatment on the acoustic emission of a compressor for the design and near surge conditions of the investigated speed line.

Methodology

The impact of the PS casing treatment on the flow and noise characteristics was established by modelling and comparing compressors with and without the casing treatment, as shown in Fig. 1. The compressor with a PS slot similar to the original configuration is referred to as the PS open configuration while the configuration without the casing treatment is called as the PS blocked configuration. This was realised by removing the PS slot in the open configuration. The acoustic characteristics of the compressor were computed using an internal or in-duct noise[14] approach wherein hydrodynamic and acoustic pressure fluctuations were calculated by directly solving the unsteady Navier-Stokes equations for each control volume of the computational domain in their conservation form using a commercial CFD coupled solver, ANSYS CFX[24].

The noise generated by the impeller was quantified using virtual pressure probes positioned in the inducer and diffuser of the compressor while the propagation of the noise was monitored by the inlet and outlet duct probes, as shown in Fig. 2. The pressure fluctuations derived from the flow solution, for the various pressure probes highlighted in Fig. 2, were processed to obtain the spectral characteristics. It is worth pointing out that the spectra of aerodynamically similar design and near surge operational states of the two compressor configurations identified in Fig. 3 were investigated to establish the impact of casing treatment.

The complete length of the inlet and outlet ducts used in the measurement rig (see Fig. 5) were not included in the model because of computational intractability, although parts of these ducts equivalent to 4 cross-sectional diameters in length were modelled. The intent of including these duct sections was to decrease the impact of the boundary conditions on the mean flow as well as to capture the flow instability that might propagate upstream of the impeller. In any case, straight ducts are used to uncouple issues due to the PS from

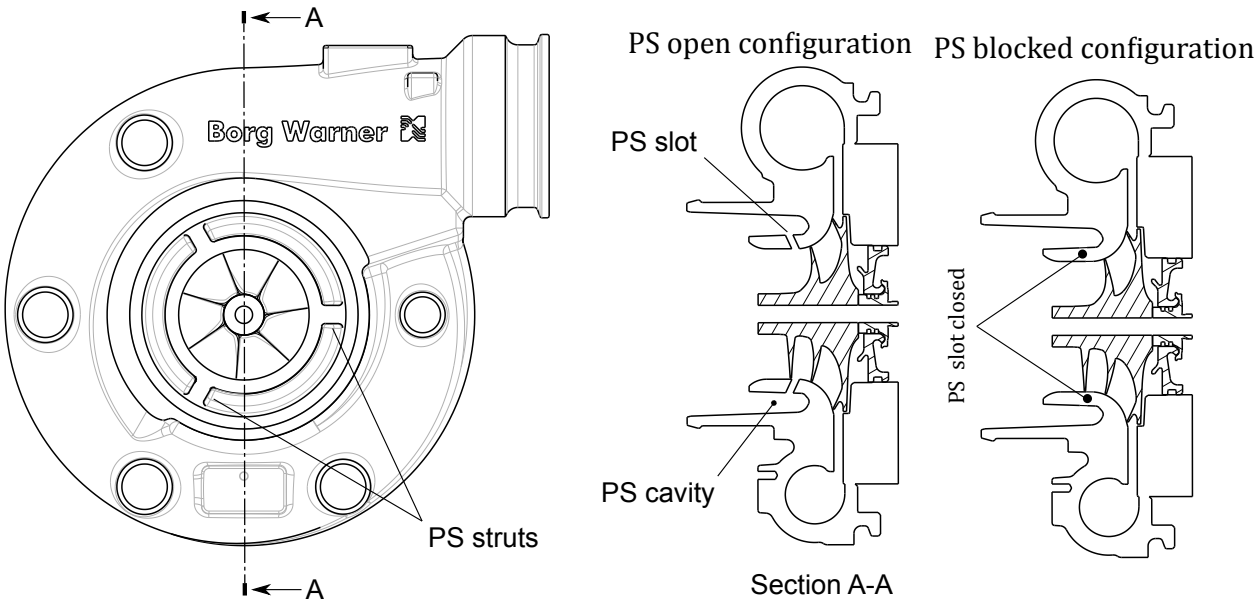

Figure 1. Drawing of the compressor along with sectional views of the open and blocked compressor configurations.

those caused by more realistic inlet geometries such as elbows,[25] tapered ducts[26] etc.

The spectra of the inducer and diffuser monitors were directly compared with the corresponding experimental probes while the duct spectra were compared using an approach presented by Broatch et al.[14] to collate the characteristics measured at different locations due to the inability to model the complete test rig. In this approach, the numerical duct spectra were computed from the decomposed pressure waves obtained by the Method of Characteristics (MoC)[27]. Furthermore, pressure wave decomposition also alleviated the issues of reflection from the duct ends and the standing waves. The pressure spectra presented in terms of Power Spectral Density (PSD) were obtained using Welch's overlapped segmented averaging[28] of the pressure data with the number of blocks selected to achieve a frequency resolution of approximately 50 Hz. Further details on the numerical modelling and methodology have been presented in Sharma et al.[12,16].

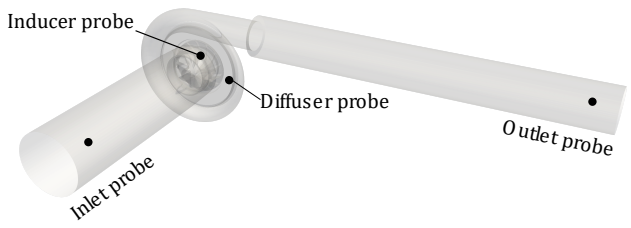

Figure 2. Computational domain along with the location of various virtual pressure probes.

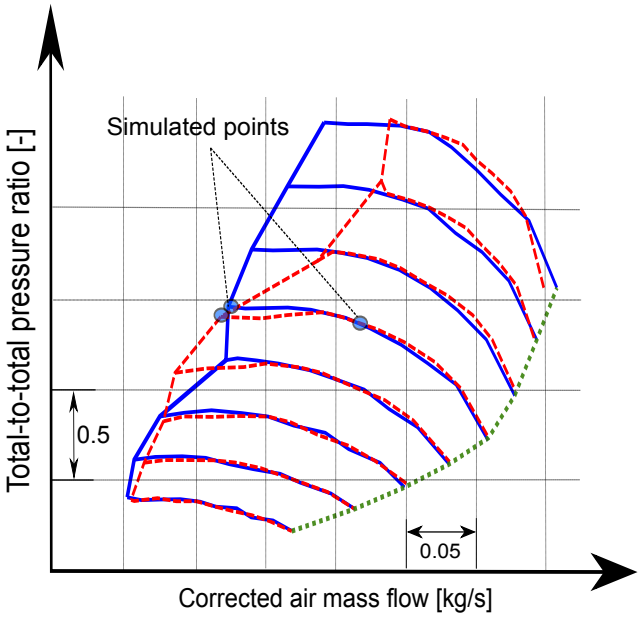

Figure 3. Experimental compressor maps for the open (blue) and blocked (red) configurations.

Numerical configuration

A B2G turbocharger PS compressor provided by industrial partner BorgWarner[29] was the subject of this investigation. The design and near surge operating conditions of the PS open and blocked configurations explored in this work are highlighted in the compressor map* presented in Fig. 3. The computational domain was spatially discretized by an unstructured polyhedral control volume created from the tetrahedral cells

*Note that this is the manufacturer-provided map; ad-hoc measurements or extrapolations[30] may be required to reach the actual deep surge line.

generated in the ICEM CFD[31] by the vertex-centered numerical approach in ANSYS CFX[24]. The grid is shown in the Fig. 4.

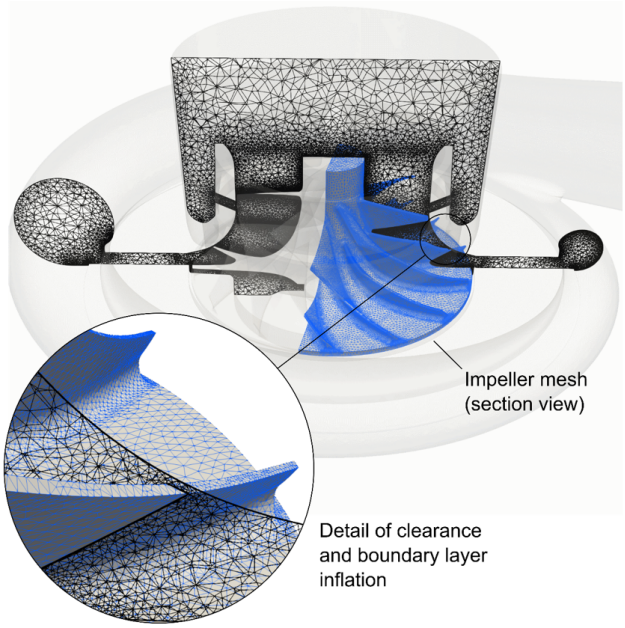

Figure 4. View of the computational domain showing a slice of the fluid mesh, the rotor surface mesh and the clearance between the blades and the shroud along with the boundary layer inflation.

This investigation focused on predicting the differences between the two compressor configurations in the ranges sensitive to the human ear (0.5-10 kHz[32]) that were observed in the experimental measurements[33]. In order to achieve this, a numerical configuration based on the Stress Blended Eddy Simulation (SBES)[34] turbulence formulation with time-steps corresponding to 4° rotation of the impeller per iteration was employed. The grid consisted of approximately 10 million cells and the boundary layer region was modelled using 12 prism layers growing exponentially with a growth ratio of 1.3 so as to obtain y^+ values closer to unity. The SBES formulation is an improvement over conventional Detached Eddy Simulation (DES), specifically in the shielding of the boundary layer and transition issues in separating shear layers[34]. The limitations of this numerical set-up which are detailed in Sharma et al.[16] include the inability to accurately capture the overall levels and decay rates. However, since this work focuses on numerically predicting the differences between the two configurations, rather than the absolute values; the aforementioned numerical set-up was the computationally optimal choice[16].

Turbulence was initialised as isotropic with curvature correction in the regions where the Reynolds averaged method was used. The working fluid in the compressor was assumed to be air behaving as a perfect gas with the ideal gas law modelling the fluid behaviour and Sutherland's law approximating the dynamic viscosity. The impeller motion was modelled using the Rigid Body Motion (RBM) approach, also known as sliding mesh in which the mesh actually rotates every time-step at the transient rotor-stator interface[24]. A steady boundary condition, as a combination of the total pressure at the inlet and mass flow rate at the outlet, was prescribed in this work. The walls were modelled as smooth with no-slip boundary conditions. As a first approach an adiabatic model was chosen, although it must be noted that models for estimating the impact of heat transfer are available[35,36] if desired.

The convective terms were discretised using a blend of second order accurate central difference scheme and first order upwind scheme to maintain the boundedness of the solution. An implicit, second-order accurate scheme implemented in ANSYS CFX[24] as the second order backward Euler scheme was used to discretise the transient terms. The hybrid model used 1% turbulent intensity and a turbulent viscosity ratio of 10 at the inlet section. Five inner coefficient loops were used for each iteration to achieve the convergence of residuals up to four orders (10^{-4}).

Assessment of the numerical configuration

The ability of the numerical configuration to yield meaningful aerodynamic and acoustic predictions was assessed by comparing numerical results with the corresponding experimental measurements. A two-step validation approach was followed in which both performance parameters and pressure spectra predicted by the numerical models were assessed against experimental data. It is worth pointing out that the variables used to compute these performance and acoustic characteristics were averaged over 1 s in the experimental measurements while numerical data was computed only up until 0.1 s of which 0.02 s was treated as an initial transient.

The performance of the PS open and blocked compressor configurations was measured at the gas stand testing facility in BorgWarner Turbo Systems, Bradford[29]. The compressor performance was characterised by measuring the thermodynamic variables of the state attained by fixing the air mass flow rate and the rotational speed of the impeller.

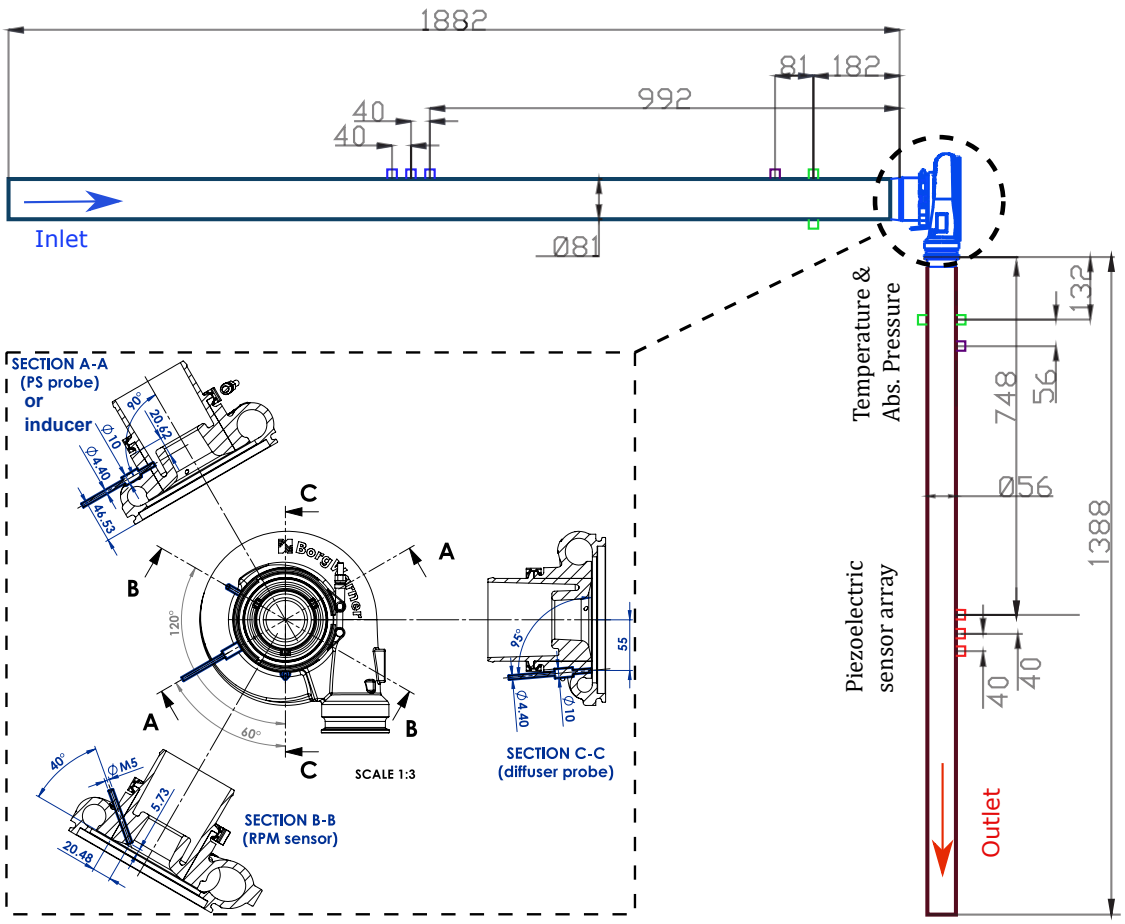

Figure 5. Experimental set-up used for acoustic measurements showing sensor positions. Dimensions in millimetres (mm).

The measured thermodynamic variables of each state were then used to compute compressor performance parameters viz. total-to-total pressure ratio Π_{t-t} and isentropic efficiency η_s as shown in Eq. 1. Further details on the gas stand measurement are described in Sharma et al.[12,37].

$$\Pi_{t-t} = \frac{p_{out,0}}{p_{in,0}}$$
$$\eta_s = \frac{\dot{W}_{is}}{\dot{W}} = \frac{T_{in,0}}{T_{out,0} - T_{in,0}} \left({\Pi_{t-t}}^{\gamma-1/\gamma} - 1 \right) \quad (1)$$

The relative difference between experimental and numerical data was quantified using a relative deviation ε value, which for a generic variable ϕ, can be defined as

$$\varepsilon = \frac{|\phi_{\text{num}} - \phi_{\text{exp}}|}{\phi_{\text{exp}}} 100 \quad (2)$$

The global performance parameters for the compressor (Eq. 1) viz. Pressure ratio Π_{t-t} and isentropic efficiency η_s along with the relative deviation from experimental values (Eq. 2) for the investigated configurations and operation are presented in Tab. 1. Although

Table 1. Comparison of the performance variables predicted by the numerical model with the experimental measurements.

Results	Configuration	Case	Π_{t-t} [-]	η_s [%]	ε_π [%]	ε_η [%]
Experimental	PS open	Design	2.35	76.8	-	-
		Near surge	2.47	66.7	-	-
	PS blocked	Design	2.37	78.5	-	-
		Near surge	2.45	68.3	-	-
Numerical	PS open	Design	2.32	76.1	1	0.9
		Near surge	2.47	66.4	0.1	0.5
	PS blocked	Design	2.33	76.3	1.6	2.8
		Near surge	2.44	66	0.4	3.3

the blocked configuration was expected to yield a higher efficiency value than the open configuration, contrary is observed in the predicted values at the near surge point. Furthermore, the deviation between the measured and predicted results, specifically for isentropic efficiency are higher for the blocked configuration. This is believed to be caused by the use of two different temperature measurement systems with different accuracy levels for the open and blocked configurations along with the slight differences in the mass flow rates for the near surge state of the two configurations. Nevertheless, the performance parameters are predicted within reasonable limits with the deviation from measured values in the range of $\pm 3\,\%$.

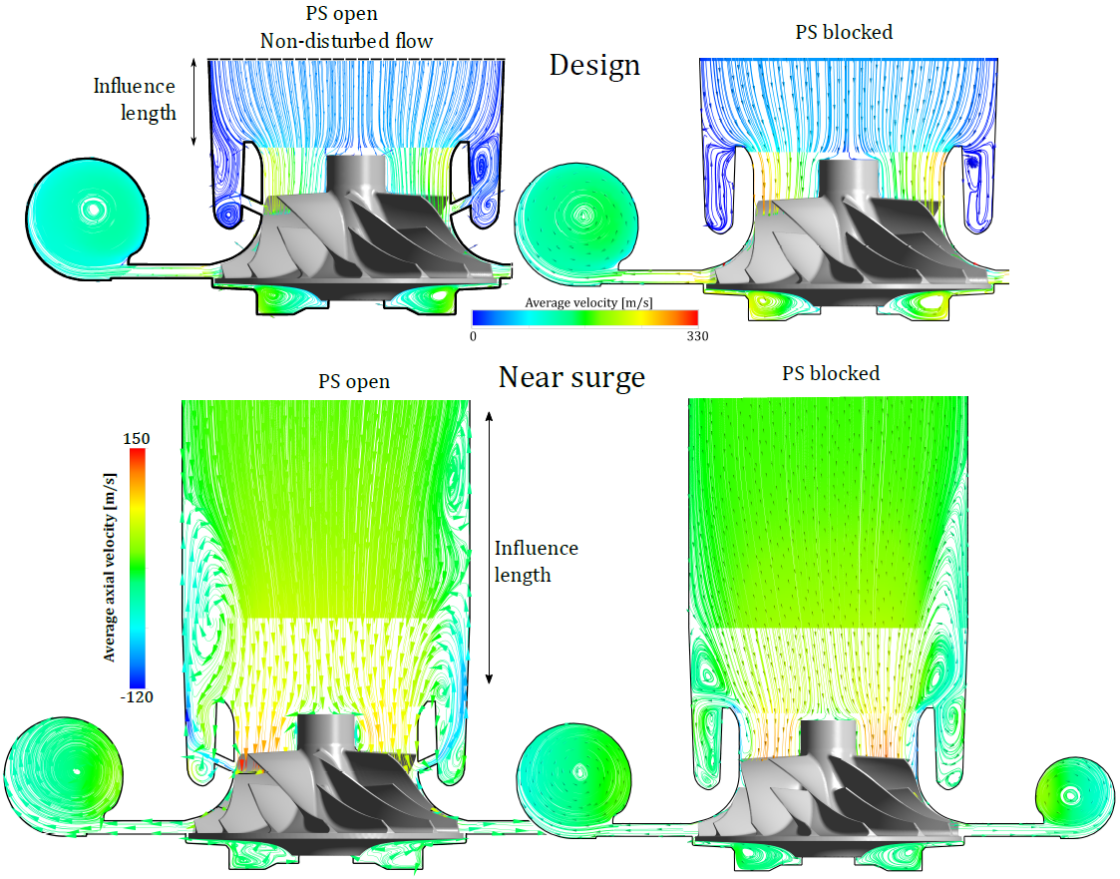

Figure 6. Comparison of the flow field characteristics for the design (top) and near surge (bottom) operation for open (left) and blocked (right) configurations.

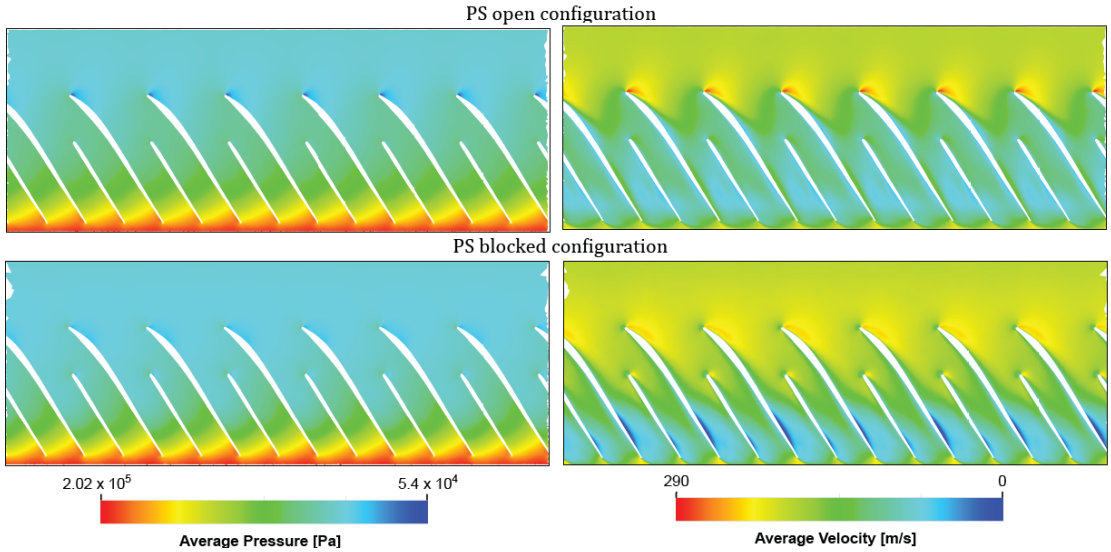

Figure 7. Midspan blade-to-blade views of average velocity (right) and average pressure (left) for open (top) and blocked (bottom) compressor configurations operating at near surge conditions.

The acoustic measurements were carried out in a flow bench facility hosted in CMT – Motores Térmicos[38]. The schematics of the test rig along with the position of various sensors is shown in Fig. 5. In addition to the sensors positioned in the inlet and outlet ducts, the instrumentation to measure the noise generated by the impeller using two miniaturised pressure probes positioned in the inducer and diffuser of the compressor are also highlighted in the figure. Further details on the flow bench and measurement methodology are already presented in Sharma et al.[33,39].

Results and discussion

The flow and acoustic features of the open and blocked compressor configurations operating near the surge and design conditions are discussed in this section.

Impact on near surge operation

In Fig. 6 (bottom), the mean flow fields on the compressor axial plane for the two compressor configurations operating near surge are presented. Although the recirculation of the flow is observed for both cases, the propagation of instability in the upstream impeller direction is higher for the open configuration. The reverse flow for the blocked configuration decreases the effective area for the incoming flow inside the impeller shroud. There is also a reduction in the upstream area caused by the flow structures. This results in a higher axial velocity at the impeller inlet for the blocked configuration compared to the open configuration.

Figure 7 shows significant differences in the average pressure and velocity distributions inside the impeller for the open and blocked configurations operating near surge. The diffusion of velocity into pressure shown in Fig. 7 (left) looks smooth and relatively uniform for the open configuration with a constant increase in the pressure along the length of the blade. Contrary to this, the increase in pressure inside the impeller is relatively abrupt in the blocked configuration and pressure rise is limited to the end of the impeller while the majority of the blade passage is observed to be at low pressure. The velocity distribution presented in Fig. 7 (right) clearly shows high-intensity blade stalls for the blocked configuration. Both main and splitter blades are observed to be in a relatively intense stall for the blocked configuration while only main blades are observed to be stalled for the open configuration. The stalling of impeller blades in the blocked configuration was further investigated by analysing the instantaneous velocity distribution in the blade passages over approximately one revolution. The velocity distribution presented in Fig. 8 clearly shows multiple (3-4) low-velocity stall cells propagating at different speeds around the impeller. For instance, blade passages 1, 2, 3 and 7 are observed to be stalled in the first time instance ($\beta°$). By following the stall in passages 5 and 6, it can be seen that the stall in passage 5 propagates circumferentially with a speed of 0.35 RO while stall in passage 6 propagates with 0.15 RO. The stalling and recovery of different blade passages can also be observed. This high intensity blade stall in the blocked configuration is expected to increase the noise emission relative to the open configuration.

The distributions of Mach number inside the impeller for the two configurations at 0.5 and 0.8 blade spans are presented in Fig. 9 (left) and Fig. 9 (middle) respectively. The significantly lower Mach number for the blocked configuration further implies detached flow and blockage inside the blade passages. This trend is observed to further deteriorate at the higher blade span.

The distribution of static entropy in the impeller mid-span region presented in Fig. 9 (right) shows higher entropy values for the blocked configuration implying greater losses compared to the open configuration. Despite lower losses in the impeller, the PS open configuration shows similar or sometimes lower isentropic efficiency when compared to the blocked configuration. This can be explained by the results of second law analysis[40] performed by Sharma et al.[37] demonstrating that the 'mixing' region accounts for higher losses in the open configuration and therefore, the interaction of recirculating flow is the leading cause for decreasing efficiency.

The generation and propagation of noise in the two compressor configurations is quantified with the help of inducer/diffuser probes and inlet/outlet duct probes respectively. The comparison of the spectra of the inducer and diffuser probes for the two configurations operating near surge are shown in Fig. 10 with the comparison of experimental results for PS open and blocked configurations shown at the top half, and the results predicted by the numerical model shown in the bottom half of the figure. Significant differences in terms of both overall levels and broadband features are evident in Fig. 10. The blocked configuration is observed to generate higher noise levels at both inducer (Fig. 10-left) and diffuser (Fig. 10-right) locations. In the measured

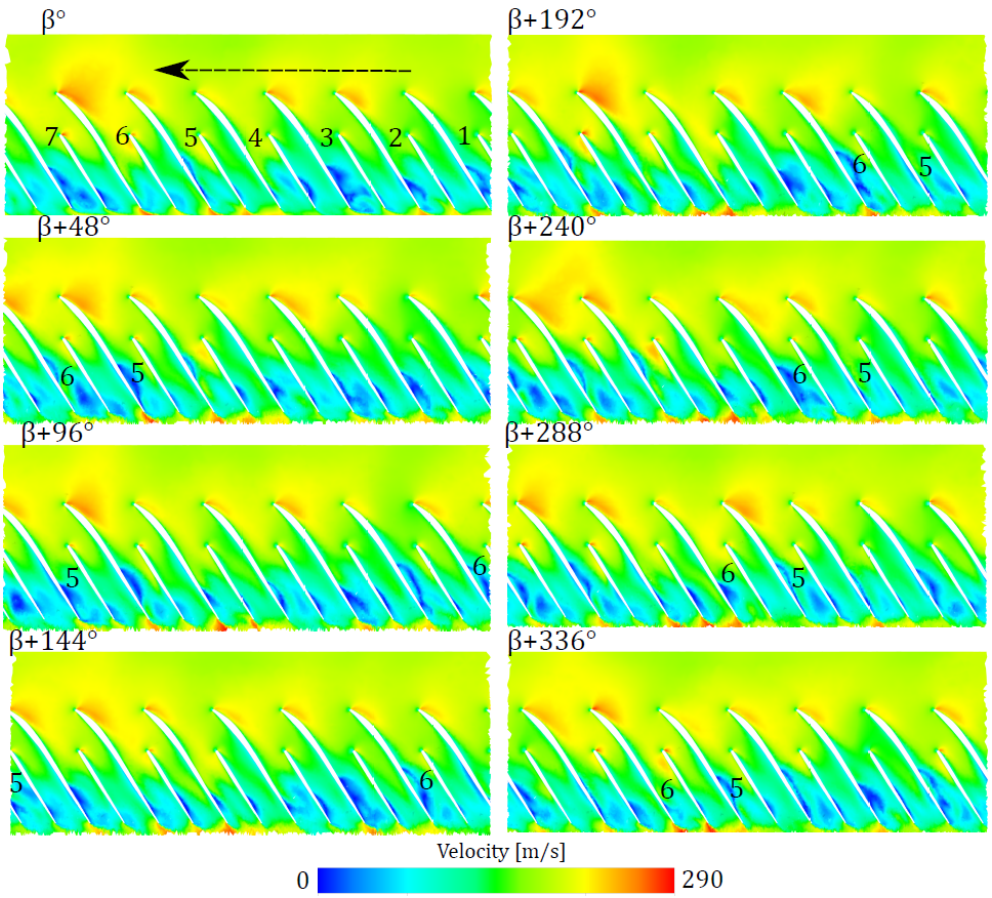

Figure 8. Instantaneous velocity distribution at impeller midspan for approximately one compressor revolution.

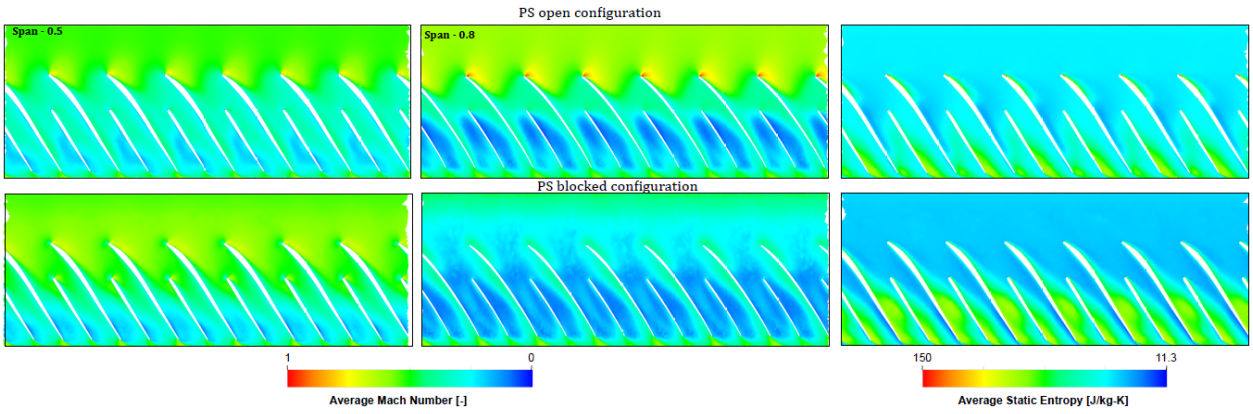

Figure 9. Blade-to-blade views of average Mach number distribution for 0.5 (left) and 0.8 (middle) blade span and average entropy generation (right) at 0.5 blade span for open (top) and blocked (bottom) compressor configurations operating at near surge conditions.

inducer spectrum, the blocked configuration is observed to yield similar or lower noise levels compared to the open configuration below 2 kHz while a broadband elevation from 2-4.5 kHz can be observed. Similarly, the diffuser spectrum for the blocked configuration also yields similar noise levels up till 0.5 kHz while a deviation in the spectra of the two configurations is observed beyond 0.5 kHz. The numerical spectra reasonably replicate these differences between the two configurations.

The inlet and outlet duct spectra for the two configurations are compared in Fig. 11. Similar to the results from the inducer probes, higher noise levels are seen beyond 2 kHz in the inlet duct of the blocked configuration while similar or lower noise levels compared to open configuration are observed below 2 kHz. It is interesting to a see a small broadband effect in the region of 0.3-0.75 kHz for the inlet duct of the open configuration which is not observed in the blocked configuration and is believed to be caused directly or

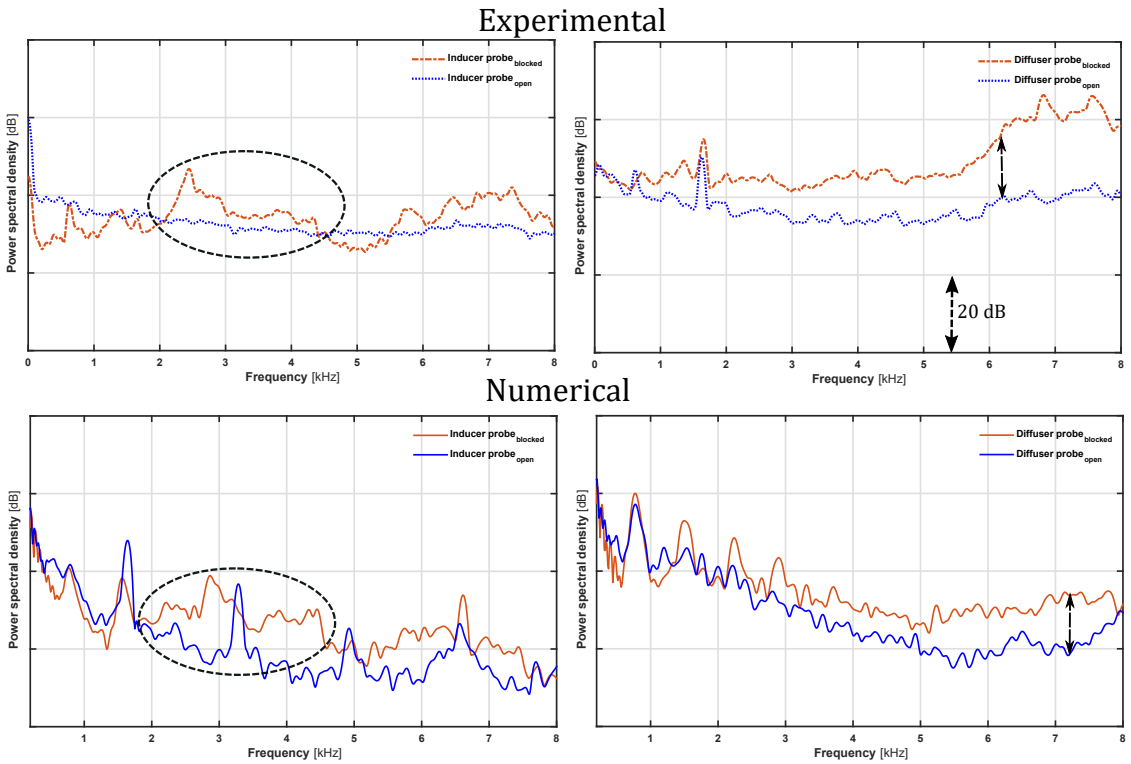

Figure 10. Experimental (top) and numerical (bottom) spectra of inducer (left) and diffuser (right) probe for open (blue) and blocked (orange) compressor configurations operating at near surge conditions.

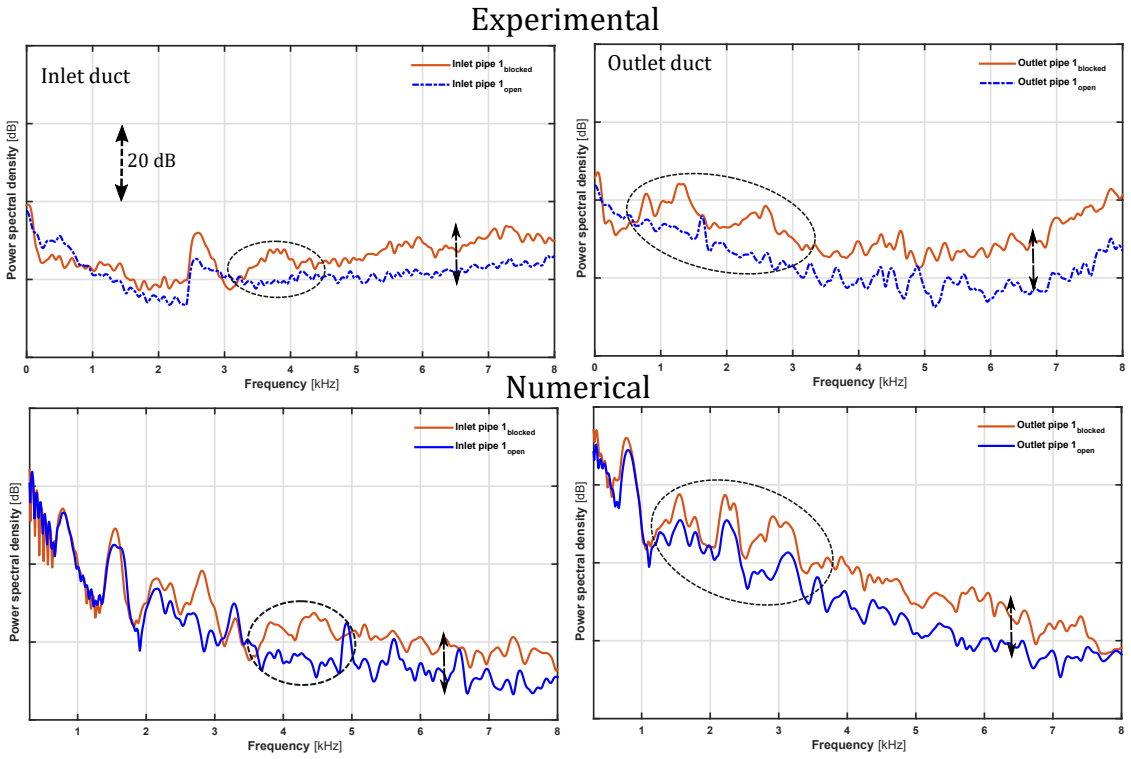

Figure 11. Experimental (top) and numerical (bottom) spectra of inlet (left) and outlet (right) ducts for open (blue) and blocked (orange) compressor configurations operating at near surge conditions.

indirectly by the casing treatment. Furthermore, the broadband in the 2-4.5 kHz region, observed in the inducer spectrum of the blocked configuration is seen to propagate to the inlet duct.

The spectra of the outlet duct are similar to the spectra of the diffuser probes with higher noise levels for the blocked configuration beyond 0.5 kHz while similar or lower levels are observed below 0.5 kHz. Broadband elevations in the region of 0.8-1.5 kHz and

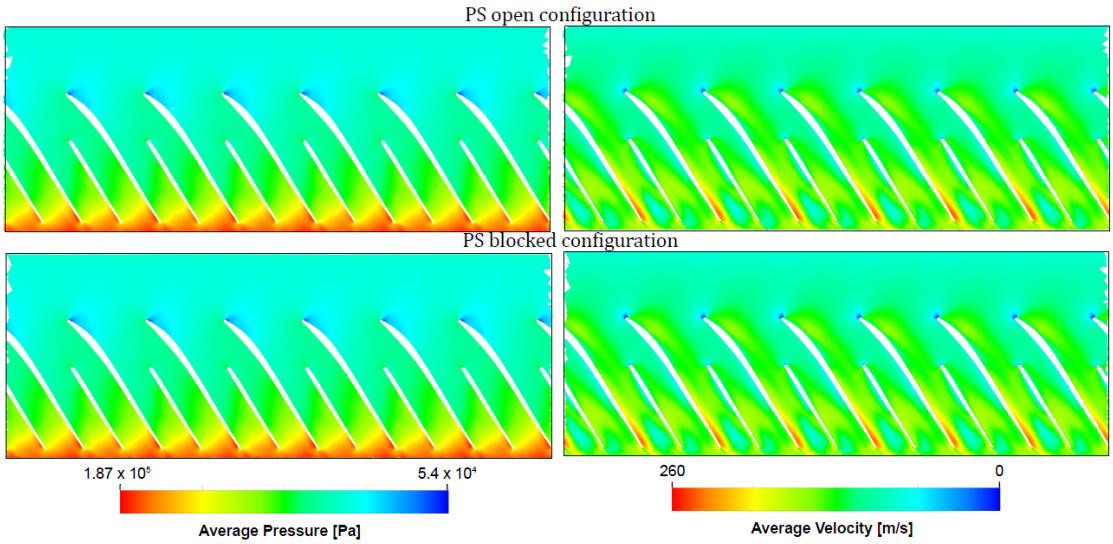

Figure 12. Midspan blade-to-blade views of average velocity (right) and average pressure (left) for open (top) and blocked (bottom) compressor configurations operating at design conditions.

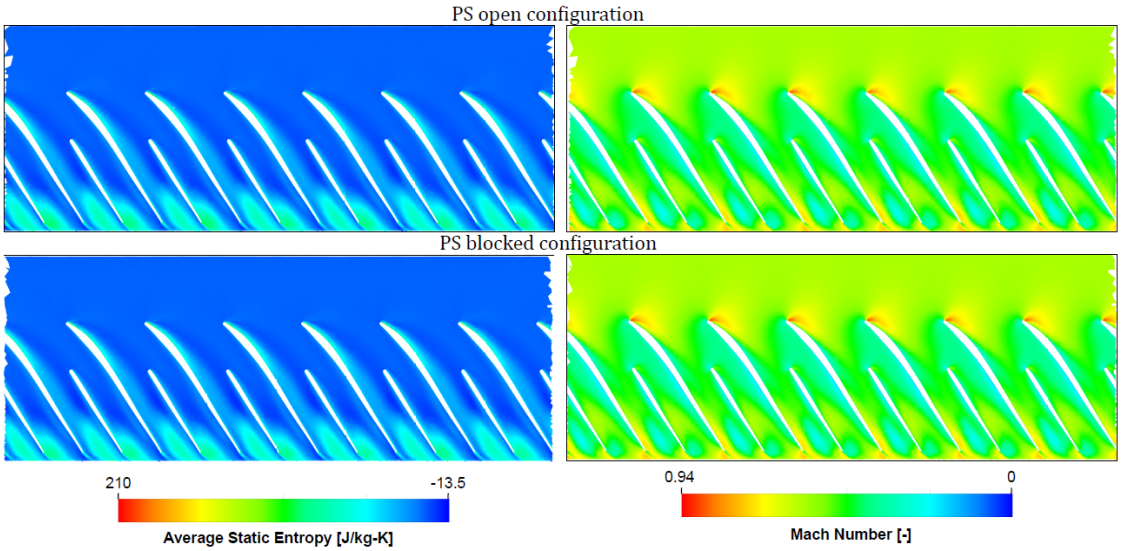

Figure 13. Midspan blade-to-blade views of average Mach number (right) and average entropy generation (left) for open (top) and blocked (bottom) compressor configurations operating at design conditions.

2-3 kHz are observed in the outlet duct of the blocked configuration that are not seen in the diffuser spectrum. The first broadband, i.e. 0.8-1.5 kHz corresponds to the characteristic 'whoosh' noise frequency range. This broadband is captured by the numerical model, and overall, numerical spectra reasonably capture the impact of casing treatment.

Impact on design operation

The mean flow field on the axial plane of the two compressor configurations operating at the design condition is shown in Fig. 6 (top). The flow in the compressor for the two configurations is similar, with a smooth reduction of the area caused by the PS cavity observed for both cases. The average velocity of the flow going into the impeller is higher in the blocked configuration as 'push and pull' on the fluid at the PS slot [12] is not present.

Although insignificant differences in the average pressure and velocity distribution inside the impeller are observed for the two cases (see Fig. 12), higher entropy and thereby losses are observed in Fig. 13 (left) for the open configuration. This higher entropy along with the losses in PS cavity corresponds to the lower isentropic efficiency for the open case as compared to the blocked case and is in line with the performance results presented in Tab. 1. Furthermore, the Mach number distribution for the two cases are also alike as observed in Fig. 13 (right).

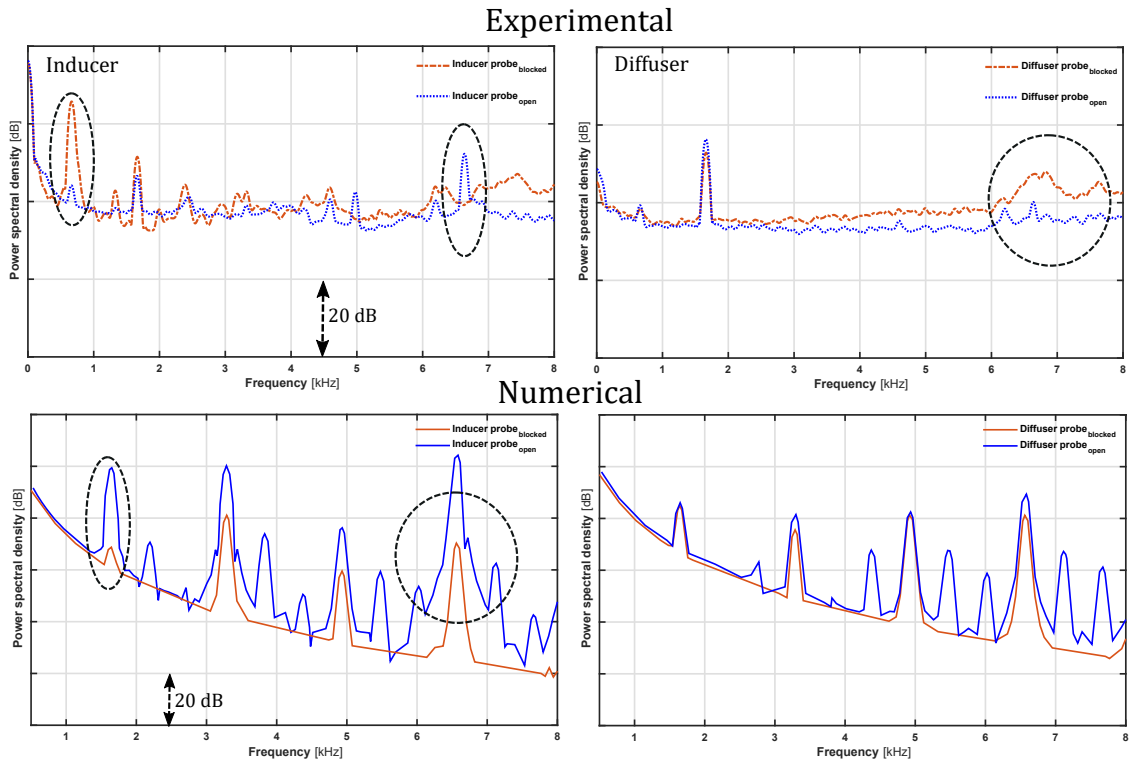

Figure 14. Experimental (top) and numerical (bottom) spectra of inducer (left) and diffuser (right) probe for open (blue) and blocked (orange) compressor configurations operating at design conditions.

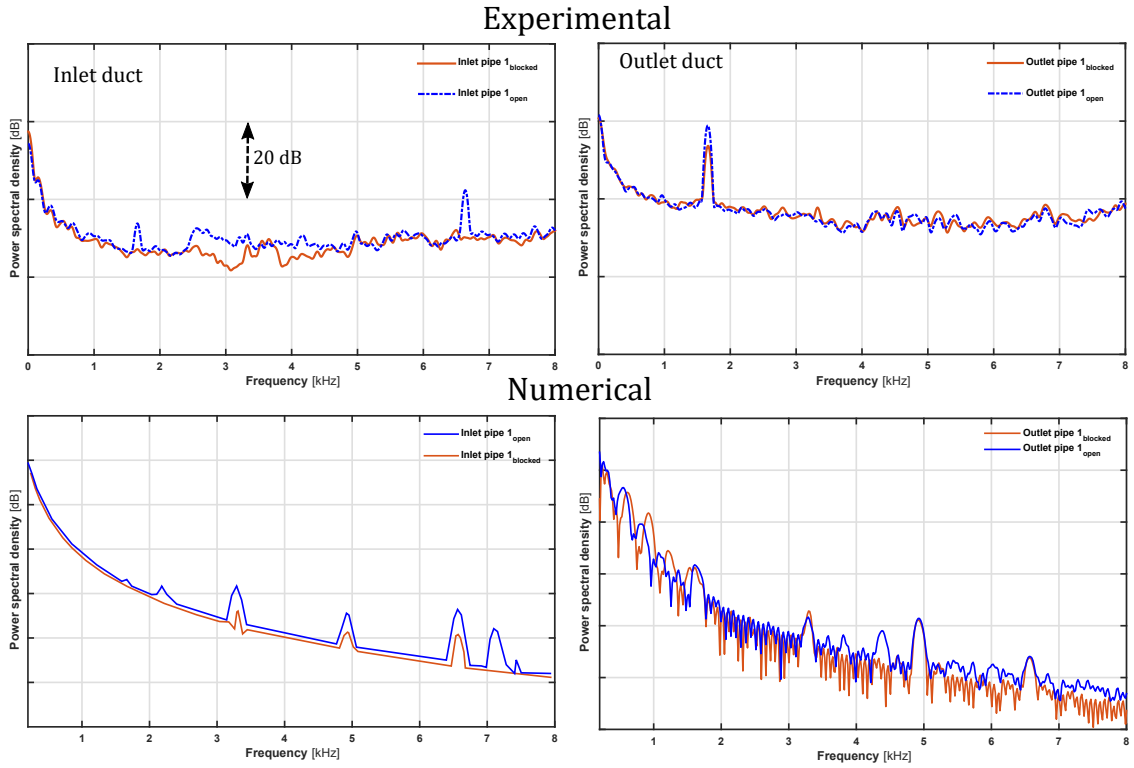

Figure 15. Experimental (top) and numerical (bottom) spectra of inlet (left) and outlet (right) ducts for open (blue) and blocked (orange) compressor configurations operating at design conditions.

The inducer and diffuser spectra for the two configurations operating at the design conditions are presented in Fig. 14. In terms of the overall noise levels, the casing treatment does not have a significant impact on the generation of the noise at design operation. This observation from the measured results is accurately captured by the numerical model. This being said, the measured inducer spectrum of the open configuration does show increased levels compared with the corresponding spectrum for the blocked

configuration at higher frequencies (see Sharma et al.[33]) which is not captured in the numerical results. The opposite trend is observed in the diffuser probes. Furthermore, the predicted spectra have accentuated tonal content relative to the measured values.

The propagation of noise at the inlet and the outlet duct for the two configurations are compared in Fig. 15. For the inlet duct, although overall levels are similar, higher tonal content is observed for the open configuration. The outlet duct spectra for the two configurations are not significantly different both in terms of overall levels and tonal content. Again, the numerical model faithfully captures these results. The higher tonal content in the inlet duct for design operation is expected due to the facilitation of noise propagation via the PS cavity. The results of the modal decomposition presented in Sharma et al.[12] further reinforces these arguments.

Conclusions

In this investigation, the impact of a ported shroud casing treatment on the acoustic and flow features of a compressor operating at the design and near surge conditions has been quantified by modelling the open and blocked configurations of the compressors. The computationally optimal numerical configuration using the SBES formulation on a grid with 10 million cells and time-steps corresponding to 4° of impeller rotation per iteration was employed. Boundary conditions were obtained through experimental testing of the selected compressor configurations. Experimental data was also used to validate the numerical model performance, demonstrating a deviation of around 3 % with respect to measurements.

The numerical spectra were shown to capture the differences between the two configurations at the investigated operating points with reasonable accuracy. Although the casing treatment was generally seen to decrease the overall acoustic emission of the compressor up to 8 kHz for both operating conditions, particular instances with the increased propagation of tonal content in the direction upstream to the impeller were observed.

For the design operation, although the flow was similar between the two configurations, higher entropy generation in the impeller region was seen for the open configuration. The acoustic spectra of inducer and diffuser probes showed slightly higher noise generation in the blocked configuration, but the propagation of noise at the inlet and outlet ducts showed insignificant differences in the overall levels of two configurations with higher tonal content in the inlet duct spectrum of open configuration.

For the near surge operation, significant differences in the flow features and therefore, acoustic features were observed for the two configurations. The diffusion of velocity into pressure was seen to be abrupt in the impeller of the blocked configuration paired with the relatively high losses evident from the entropy generation. These losses are attributed to the intense stall observed in multiple blade passages of the blocked configuration. The blocked compressor was seen to generate higher flow-induced noise compared to the open configuration. Both inducer and diffuser spectra showed similar or lower noise levels for lower frequencies while significantly higher levels were observed beyond those cut-off frequencies for the blocked configuration. Broadband characteristics in the lower and medium frequency regions usually associated with near surge operation were observed in the spectra of the blocked configuration. Furthermore, broadbands in the characteristic ‘whoosh’ noise frequency were also seen in the spectrum of the outlet duct for the blocked configuration.

Acknowledgements

The project is sponsored and supported by BorgWarner Turbo Systems and the Regional Growth Fund (RGF Grant Award 01.09.07.01/1789C). The authors would like to thank BorgWarner Turbo Systems for permission to publish the results presented in this paper. The support of the HPC group at the University of Huddersfield is gratefully acknowledged.

Declaration of conflicting interests

The author(s) declared no potential conflicts of interest with respect to the research, authorship, and/or publication of this article.

Nomenclature

List of symbols

T temperature (K)

$T_{\text{out},0}$ total temperature at the outlet boundary (K)

$\dot{W}$ compressor absorbed work ($\mathrm{kgm^2s^{-3}}$)

ε relative deviation (%)

γ ratio of specific heats (−)

ϕ generic variable

$p_{\mathrm{out},0}$ total pressure at the outlet boundary (Pa)

$\Pi_{\mathrm{t\text{-}t}}$ total-to-total pressure ratio (-)

η_s isentropic efficiency (-)

y^+ dimensionless wall distance (-)

List of abbreviations

BPF blade passing frequency (Hz)

CFD computational fluid dynamics

DES detached eddy simulation

PIV particle-imaging velocimetry

PS ported shroud

PSD pressure spectral density (dB)

RBM rigid body motion

SBES stress-blended eddy simulation

TCN tip clearance noise

References

1. Macdougal I and Elder R. The improvement of operating range in a small, high speed, centrifugal compressor using casing treatment. In IMechE Conference on Turbochargers and Turbocharging, Paper. C32/82.
2. Eynon P, Whitfield A, Firth M et al. A study of the flow characteristics in the inducer bleed slot of a centrifugal compressor. In ASME 1996 International Gas Turbine and Aeroengine Congress and Exhibition. American Society of Mechanical Engineers. DOI:10.1115/96-GT-262.
3. Fisher F. Application of map width enhancement devices to turbocharger compressor stages. Technical report, SAE Technical Paper, 1988. DOI:10.4271/880794.
4. Cheng L, Dimitriou P, Wang W et al. A novel fuzzy logic variable geometry turbocharger and exhaust gas recirculation control scheme for optimizing the performance and emissions of a diesel engine. International Journal of Engine Research 2018; DOI: 10.1177/1468087418809261.
5. Semlitsch B, JyothishKumar V, Mihaescu M et al. Numerical flow analysis of a centrifugal compressor with ported and without ported shroud. Technical report, SAE Technical Paper, 2014. DOI:10.4271/2014-01-1655.
6. Teng C and Homco S. Investigation of compressor whoosh noise in automotive turbochargers. SAE International Journal of Passenger Cars-Mechanical Systems 2009; 2(2009-01-2053): 1345–1351. DOI:10.4271/2009-01-2053.
7. Evans D and Ward A. Minimising turbocharger whoosh noise for diesel powertrains. Technical report, SAE Technical Paper, 2005. DOI:10.4271/2005-01-2485.
8. Trochon EP. A new type of silencers for turbocharger noise control. Technical report, SAE Technical Paper, 2001. DOI:10.4271/2001-01-1436.
9. Figurella N, Dehner R, Selamet A et al. Noise at the mid to high flow range of a turbocharger compressor. Noise Control Engineering Journal 2014; 62(5): 306–312. DOI: 10.3397/1/376229.
10. Raitor T and Neise W. Sound generation in centrifugal compressors. Journal of Sound and Vibration 2008; 314(3): 738–756. DOI:10.1016/j.jsv.2008.01.034.
11. Tiikoja H, Rämmal H, Abom M et al. Investigations of automotive turbocharger acoustics. SAE International Journal of Engines 2011; 4(2): 2531–2542. DOI:10.4271/2011-24-0221.
12. Sharma S, Broatch A, Garcıa-Tıscar J et al. Acoustic characteristics of a ported shroud turbocompressor operating at design conditions. International J of Engine Research 2018; 1: 15. DOI:10.1177/1468087418814635.
13. Mendonça F, Baris O and Capon G. Simulation of radial compressor aeroacoustics using CFD. In Proceedings of ASME Turbo Expo. pp. 1823–1832. DOI:10.1115/GT2012-70028.
14. Broatch A, Galindo J, Navarro R et al. Methodology for experimental validation of a CFD model for predicting noise generation in centrifugal compressors. International Journal of Heat and Fluid Flow 2014; 50: 134–144. DOI:10.1016/j.ijheatfluidflow.2014.06.006.
15. Broatch A, García-Tíscar J, Roig F et al. Dynamic mode decomposition of the acoustic field in radial compressors. Aerospace Science and Technology 2019; 90: 388–400. DOI:10.1016/j.ast.2019.05.015.

16. Sharma S, Garcıa-Tıscar J, Allport JM et al. Evaluation of modelling parameters for computing flow-induced noise in a small high-speed centrifugal compressor. Submitted to Aerospace Science and Technology 2019; .
17. Sundström E, Semlitsch B and Mihăescu M. Generation mechanisms of rotating stall and surge in centrifugal compressors. Flow, Turbulence and Combustion 2018; 100(3): 705–719. DOI:10.1007/s10494-017-9877-z.
18. Sundström E, Semlitsch B and Mihăescu M. Acoustic signature of flow instabilities in radial compressors. Journal of Sound and Vibration 2018; 434: 221–236. DOI:10.1016/j.jsv.2018.07.040.
19. Guillou E, Dimicco R, Gutmark E et al. Characterization of a ported shroud compressor using piv measurements. SAE Technical Papers 2010; DOI:10.4271/2010-01-1225.
20. Chen H and Yin J. Turbocharger compressor development for diesel passenger car applications. In IMechE Eighth International Conference on Turbochargers and Turbocharging, London, May. pp. 17–18. DOI:10.1016/B978-1-84569-174-5.50005-1.
21. Chen H and Lei VM. Casing treatment and inlet swirl of centrifugal compressors. Journal of Turbomachinery 2013; 135(4): 041010.
22. Dehner R, Selamet A, Steiger M et al. The Effect of Ported Shroud Recirculating Casing Treatment on Turbocharger Centrifugal Compressor Acoustics, volume 10. 2017. DOI:10.4271/2017-01-1796.
23. Fardafshar N and Koutsovasilis P. Ported Shroud Influence on the Aero-Acoustic Properties of Automotive Turbochargers: Quantification by Means of Simulation and Measurement. 2018.
24. CFX-Solver A. Theory guide. Release ll 2006; .
25. Song K, Zhao B, Sun H et al. A physics-based zero-dimensional model for the mass flow rate of a turbocharger compressor with uniform/distorted inlet condition. International Journal of Engine Research 2018; DOI:10.1177/1468087418773673.
26. Broatch A, Margot X, García-Tíscar J et al. Impact of simple surge-enhancing inlet geometries on the acoustic behavior of a turbocompressor. International Journal of Engine Research 2018; DOI:10.1177/1468087418784125.
27. Torregrosa A, Fajardo P, Gil A et al. Development of non-reflecting boundary condition for application in 3d computational fluid dynamics codes. Engineering Applications of Computational Fluid Mechanics 2012; 6(3): 447–460. DOI:10.1080/19942060.2012.11015434.
28. Welch P. The use of fast fourier transform for the estimation of power spectra: A method based on time averaging over short, modified periodograms. IEEE Transactions on Audio and Electroacoustics 1967; 15(2): 70–73. DOI:10.1109/TAU.1967.1161901.
29. Systems BT. Bradford, uk. URL http://turbos.borgwarner.com.
30. Galindo J, Navarro R, García-Cuevas LM et al. A zonal approach for estimating pressure ratio at compressor extreme off-design conditions. International Journal of Engine Research 2019; 20(4): 393–404. DOI:10.1177/1468087418754899.
31. ANSYS I and ANSYS I. Cfd help manual. ANSYS, Inc, Canonsburg, PA 2012; .
32. Gelfand SA. Essentials of audiology. New York: Thieme, 2007, 2007.
33. Sharma S, Broatch A, Garcıa-Tıscar J et al. Acoustic characterisation of a small high-speed centrifugal compressor with casing treatment: An experimental study. Submitted to Aerospace Science and Technology 2019; .
34. Menter F. Stress-blended eddy simulation (sbes)—a new paradigm in hybrid rans-les modeling. In Symposium on Hybrid RANS-LES Methods. Springer, pp. 27–37.
35. Serrano JR, Olmeda P, Arnau FJ et al. A holistic methodology to correct heat transfer and bearing friction losses from hot turbocharger maps in order to obtain adiabatic efficiency of the turbomachinery. International Journal of Engine Research 2019; DOI:10.1177/1468087419834194.
36. Gil A, Tiseira AO, García-Cuevas LM et al. Fast three-dimensional heat transfer model for computing internal temperatures in the bearing housing of automotive turbochargers. International Journal of Engine Research 2018; DOI:10.1177/1468087418804949.
37. Sharma S, Jupp ML, Nickson AK et al. Ported shroud flow processes and their effect on turbocharger compressor operation. In ASME Turbo Expo 2017: Turbomachinery Technical Conference and Exposition. American Society of Mechanical Engineers, pp. V02CT44A017–V02CT44A017. DOI:10.1115/GT2017-63678.
38. Térmicos CM. Universitat politècnica de València, 1979. URL https://www.cmt.upv.es/.
39. Sharma S, Broatch A, García-Tíscar J et al. Acoustic and pressure characteristics of a ported shroud turbocompressor operating at near surge conditions. Applied Acoustics 2019; 148: 434–447. DOI:10.1016/j.apacoust.2019.01.005.
40. Herwig H and Schmandt B. How to determine losses in a flow field: A paradigm shift towards the second law analysis. Entropy 2014; 16(6): 2959. DOI:10.3390/

e16062959.